Journal of Advanced Research 54 (2023) 29–42

Contents lists available at ScienceDirect

Journal of Advanced Research

journal homepage: www.elsevier.com/locate/jare

Original Article

LncRNA *NIPA1-SO* confers atherosclerotic protection by suppressing the transmembrane protein NIPA1

Min Jiang [a,1], Yu Song [a,1], Mei-Xia Ren [b,c,1], Run-Chao He [a], Xian-Hui Dong [a], Xue-Heng Li [d], Zhi-Feng Lu [d], Shu Li [a], Jia Wu [a], Yan-Rou Bei [d], Fei Liu [a], Yan Long [a], Shao-Guo Wu [e], Xue-Hui Liu [e], Li-Mei Wu [e], Hong-Ling Yang [a], David G. McVey [f], Xiao-Yan Dai [g,*], Shu Ye [h,i,*], Yan-Wei Hu [a,d,*]

[a] *Department of Clinical Laboratory, Guangzhou Women & Children Medical Center, Guangzhou Medical University, Guangzhou 510620, China*
[b] *Shengli Clinical Medical College of Fujian Medical University, Fujian Medical University, Fuzhou 350001, China*
[c] *Department of Geriatric Medicine, Fujian Provincial Hospital, Fujian Key Laboratory of Geriatrics, Fujian Provincial Center for Geriatrics, Fuzhou 350013, China*
[d] *Laboratory Medicine Center, Nanfang Hospital, Southern Medical University, Guangzhou 510515, China*
[e] *Department of Clinical Laboratory, Guangzhou Twelfth People's Hospital, Guangzhou 510620, China*
[f] *Department of Cardiovascular Sciences & NIHR Leicester Biomedical Research Centre, University of Leicester, Leicester LE3 9QP, UK*
[g] *Key Laboratory of Molecular Target & Clinical Pharmacology and the State Key Laboratory of Respiratory Disease, School of Pharmaceutical Sciences, Guangzhou Medical University, Guangzhou, Guangdong 511436, China*
[h] *Cardiovascular Translational Research Programme, National University of Singapore, Singapore*
[i] *Shantou University Medical College, Shantou, China*

HIGHLIGHTS

- Human atherosclerotic plaques have reduced expression of the long non-coding RNA NIPA1-SO and increased levels of NIPA1.
- NIPA1-SO inhibits monocyte adhesion to endothelial cells and decreases cholesterol accumulation.
- Increasing the expression of NIPAI-SO

GRAPHICAL ABSTRACT

Schematic diagram of the signalling pathways regulated by *NIPA1-SO*. Our study has uncovered an athero-protective role of the lncRNA *NIPA1-SO*, which, by interacting with a single transcription factor, is capable of inhibiting monocyte adhesion and foam cell formation, two fundamental processes in atherosclerosis. The transcription factor FUBP1 negatively regulates NIPA1 expression; this inhibitory effect is increased by the interaction of *NIPA1-SO* with FUBP1, resulting in lower transcription of NIPA1. A reduction in NIPA1 protein results in increased BMPR2 protein due to a reduction in NIPA1-mediated BMPR2 endocytosis and degradation, leading to higher levels of Smad1/5/8 phosphorylation (pSmad1/5/8), which, through complexation with Smad4, inhibit transcription of the adhesion molecules

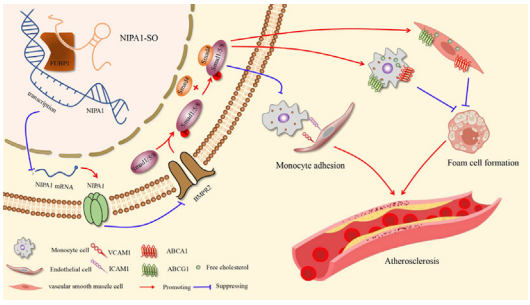

Peer review under responsibility of Cairo University.

* Corresponding authors at: Department of Clinical Laboratory, Guangzhou Women & Children Medical Center, Guangzhou Medical University, Guangzhou 510620, China (W. Hu). Cardiovascular Translational Research Programme, National University of Singapore, Singapore (S. Ye). Key Laboratory of Molecular Target & Clinical Pharmacology and the State Key Laboratory of Respiratory Disease, School of Pharmaceutical Sciences, Guangzhou Medical University, Guangzhou, Guangdong 511436, China (X. Dai).
E-mail addresses: xdai@gzhmu.edu.cn (X.-Y. Dai), sy127@leicester.ac.uk (S. Ye), ywhu0618@163.com (Y.-W. Hu).

[1] These authors contributed equally to this work.

https://doi.org/10.1016/j.jare.2023.01.017
2090-1232/

or knockout of NIPA1 reduces atherosclerosis in an animal model. VCAM1 and ICAM1, reducing monocyte adhesion to endothelial cells. Further, the pSmad1/5/8:Smad4 complex promotes ABCA1 and ABCG1 transcription, both of which promote cholesterol efflux via high-density lipoprotein (HDL) particles, thereby inhibiting foam cell formation.

ARTICLE INFO

Article history:
Received 6 April 2022
Revised 10 October 2022
Accepted 20 January 2023
Available online 2 February 2023

Keywords:
Atherosclerosis
LncRNA
NIPA1
Vascular adhesion molecule

ABSTRACT

Long non-coding RNAs (lncRNAs) are emerging as important players in gene regulation and cardiovascular diseases. However, the roles of lncRNAs in atherosclerosis are poorly understood. In the present study, we found that the levels of *NIPA1-SO* were decreased while those of NIPA1 were increased in human atherosclerotic plaques. Furthermore, *NIPA1-SO* negatively regulated NIPA1 expression in human umbilical vein endothelial cells (HUVECs). Mechanistically, *NIPA1-SO* interacted with the transcription factor FUBP1 and the *NIPA1* gene. The effect of *NIPA1-SO* on NIPA1 protein levels was reversed by the knockdown of *FUBP1*. *NIPA1-SO* overexpression increased, whilst *NIPA1-SO* knockdown decreased BMPR2 levels; these effects were enhanced by the knockdown of *NIPA1*. The overexpression of *NIPA1-SO* reduced while *NIPA1-SO* knockdown increased monocyte adhesion to HUVECs; these effects were diminished by the knockdown of *BMPR2*. The lentivirus-mediated-overexpression of *NIPA1-SO* or gene-targeted knockout of *NIPA1* in low-density lipoprotein receptor-deficient mice reduced monocyte-endothelium adhesion and atherosclerotic lesion formation. Collectively, these findings revealed a novel anti-atherosclerotic role for the lncRNA *NIPA1-SO* and highlighted its inhibitory effects on vascular inflammation and intracellular cholesterol accumulation by binding to FUBP1 and consequently repressing *NIPA1* expression.

Introduction

Long non-coding RNAs (lncRNAs), defined as gene transcripts of ≥200 nucleotides in length that are not translated into proteins, can modulate the expression of protein-coding genes and consequently affect cell behavior [1]. Several lncRNAs have been implicated in the pathogenesis of atherosclerosis [2]. The biological functions of many lncRNAs, however, are still unknown.

The non-imprinted in Prader-Willi/Angelman Syndrome region protein 1 (*NIPA1*) gene is highly expressed in the brain, and mutations in this gene have been implicated in the development of an autosomal dominant form of hereditary spastic paraplegia (HSP) [3–5]. Transmembrane protein NIPA1 can function as a Mg^{2+} transporter and control Mg^{2+} uptake; this is the basis for HSP [6]. The deficiency of four highly-conserved and non-imprinted genes, namely *NIPA1*, *NIPA2*, *CYFIP1*, *TUBGCP5*, was previously associated with congenital heart disease [7]. Recently, emerging evidence showed a significant upregulation of *NIPA1* gene expression in pulmonary arterial smooth muscle cells (PASMCs) during chronic hypoxia and monocrotaline-induced pulmonary hypertension, a life-threatening pulmonary vascular disease in humans [8]. However, whether and how NIPA1 plays a role in atherosclerosis remains to be elucidated.

Here, we report that the lncRNA *NIPA1-SO*, whose function was previously unknown, modulated the expression of the transmembrane magnesium transporter protein NIPA1, and that *NIPA1-SO* affected monocyte adhesion to vascular endothelial cells and intracellular cholesterol level in a BMPR2-dependent manner. Furthermore, using a well-established mouse model of atherosclerosis, we demonstrated that augmenting *NIPA1-SO* expression or abolishing NIPA1 could inhibit atherogenesis.

Results

Human atherosclerotic plaques exhibit reduced NIPA1-SO and increased NIPA1 expression

We previously performed differential expression analysis of human atherosclerotic tissues in comparison with normal arterial specimens using Arraystar LncRNA Expression Microarray V3.0, which contained probes for 24,748 lncRNAs and 24,420 protein-coding transcripts. This analysis detected a number of differentially expressed lncRNAs (Appendix Fig. S1A and data file S1) and mRNAs (Appendix Fig. S2A and data file S2), some of which have been described recently [9–11]. One of the most significantly downregulated lncRNA in atherosclerotic plaques was ENSG00000274253 (*LOC283683*, referred to here as *NIPA1-SO* standing for *NIPA1* sense overlapping); the expression level of this gene was 43.29 ± 0.06-f old lower in human atherosclerotic plaques than in normal intimal tissues ($P < 0.001$) (Appendix Fig. S1A and B, and data file S1). The gene encoding *NIPA1-SO* was located at nucleotide position 23,094,330 to 23,115,254 on chromosome 15 (GRCh37/hg19) and overlapped with the *NIPA1* gene which was located at position 23,043,278–23,086,843. Interestingly, the level of *NIPA1* expression was significantly higher in atherosclerotic plaques than in normal intimal tissues (a 13.67 ± 0.08-fold difference, $P < 0.001$) (Appendix Fig. S2A-C, and data file S2). Subsequent analyses using quantitative reverse transcription polymerase chain reaction (RT-PCR), fluorescence in situ hybridization, Western blotting, and immunohistochemistry, confirmed that *NIPA1-SO* expression was decreased, whilst NIPA1 was increased, in atherosclerotic plaques (Fig. 1A-D).

Quantitative RT-PCR analyses showed that the expression level of *NIPA1-SO* in human atherosclerotic plaques was approximately 0.05% relative to the expression level of the housekeeping gene *GAPDH* (Appendix Fig. S3A) and that cultured human umbilical vein endothelial cells (HUVECs), THP-1 cells, and human aortic smooth muscle cells (HASMCs) contained approximately 15, 8, and 7.5 copies of *NIPA1-SO* per cell, respectively (Appendix Fig. S3B). Our experiments further indicated that *NIPA1-SO* did not contain a poly-A tail (Appendix Fig. S3C) and that *NIPA1-SO* was present in both the nucleus and cytoplasm of HUVECs (Fig. 1E).

NIPA1-SO downregulates NIPA1 expression

Double immunostaining studies of atherosclerotic arterial tissues showed that NIPA1 was expressed in endothelial cells (ECs, identified by positive staining for the endothelial cell marker

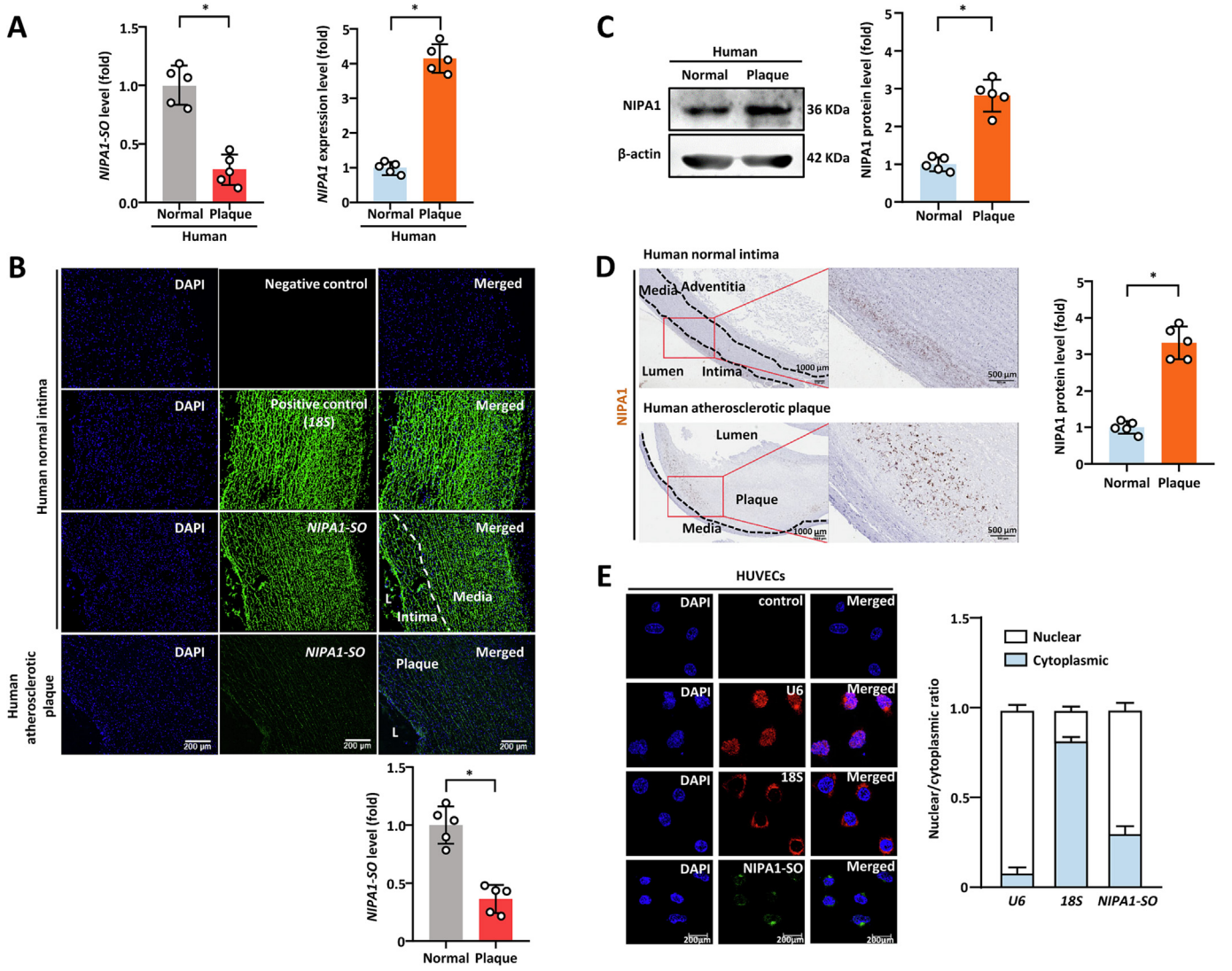

Fig. 1. *NIPA1-SO* and NIPA1 are differentially expressed in human normal and atherosclerotic tissues. (**A**) Expression of *NIPA1-SO* and *NIPA1* were assessed via RT-PCR in both human normal and atherosclerotic plaque tissues. Data are presented following normalization to either U6 RNA (*NIPA1-SO*) or *GAPDH* (*NIPA1*) and to the normal carotid tissue samples using the ΔΔCt method (n = 5). (**B**) FISH analysis of human normal and atherosclerotic tissue samples. Green fluorescence shows expression of *NIPA1-SO* whilst blue fluorescence indicates nuclei stained with the DNA stain DAPI (n = 5). Scale bar = 200 μm. (**C**) Western blotting of NIPA1 protein levels in human normal and plaque tissues (n = 5). Protein levels were normalized to β-actin and to the levels of expression in normal tissue. (**D**) Immunohistochemistry of human normal and atherosclerotic carotid artery tissue samples to examine NIPA1 expression (brown). Data shown are normalized to normal intima tissue samples (n = 5). (**E**) Fluorescence in situ hybridization was employed to determine the intracellular locations of *NIPA1-SO* in cultured human umbilical vein endothelial cells (HUVECs). *NIPA1-SO* was stained green with RNA probes, while 18S (a cytoplasmic marker) and U6 (a nuclear marker) were stained red with fluorescent secondary antibody (n = 3). $^{*}P < 0.05$ by unpaired 2-tailed Student's *t*-test. (For interpretation of the references to color in this figure legend, the reader is referred to the web version of this article.)

CD34), monocytes/macrophages (MΦs, positive staining for LGALS3), and vascular smooth muscle cells (VSMCs, positive staining for α-smooth muscle actin) (Fig. 2A).

Because lncRNAs can regulate the expression of nearby genes [1], we investigated whether *NIPA1-SO* modulated *NIPA1* expression. We transduced cultured HUVECs, THP-1 cells, and HASMCs with either an shRNA to knockdown *NIPA1-SO* or a lentivirus to increase *NIPA1-SO* expression. Cells with lentivirus-mediated overexpression of *NIPA1-SO* had reduced NIPA1 expression compared to cells transduced with a control lentivirus vector (Fig. 2B and C) while cells with shRNA-mediated knockdown of *NIPA1-SO* showed increased NIPA1 expression when compared to transduction with a control shRNA (Fig. 2D), thus suggesting a down-regulatory effect of *NIPA1-SO* on NIPA1 expression. In addition, RNA-sequencing of cultured HUVECs transduced with either a *NIPA1-SO* expressing lentivirus or the lentivirus vector (control) confirmed that *NIPA1-SO* could inhibit *NIPA1* expression (Appendix Fig. S4A, B, and data file S5).

To investigate whether *NIPA1-SO* interacted with the *NIPA1* gene, we performed chromatin isolation by RNA purification (ChIRP) analysis [12] using *NIPA1-SO* RNA probes to pull down chromatin in cultured HUVECs. Next, we performed PCR using the pulled-down DNA as template and primers annealing to the *NIPA1* gene promoter. Analysis detected *NIPA1* in the chromatin DNA pulled down by the *NIPA1-SO* RNA probes, thus suggesting that *NIPA1-SO* interacted with the *NIPA1* gene (Appendix Fig. S6). In comparison, the negative controls *GAPDH* and *ACTB* were barely detectable in the pulldown by the *NIPA1-SO* RNA probes; *NIPA1* was barely detectable in chromatin DNA pulled down by a *LacZ* probe serving as a negative control (Appendix Fig S6).

Mass spectrometry analysis of the chromatin pulled down by the *NIPA1-SO* RNA probes detected the presence of a number of proteins, five of which have reported properties: (1) nuclear location, (2) single-stranded DNA binding, (3) mRNA binding, (4) positive regulation of gene regulation, and (5) RNA binding (Fig. 3A).

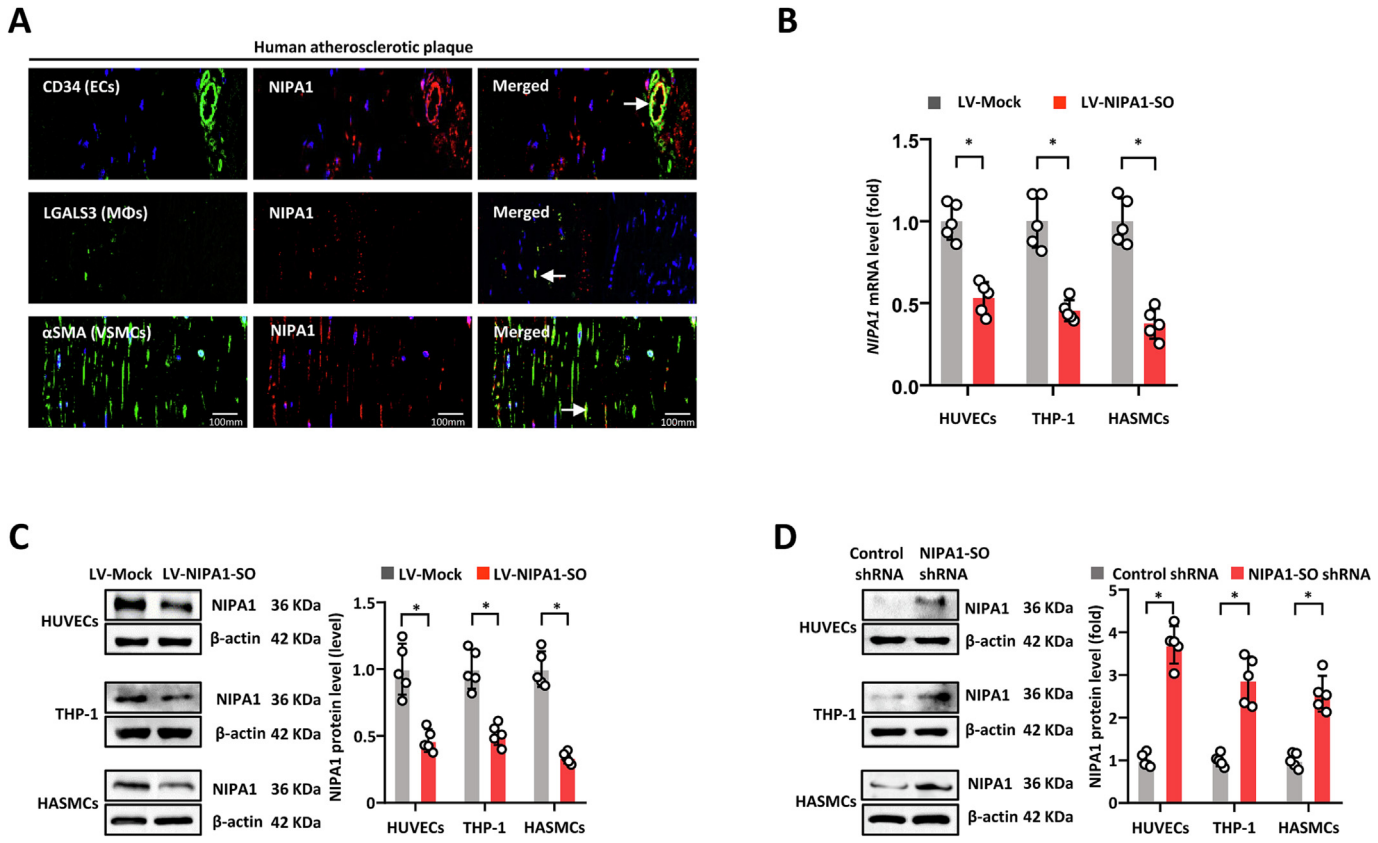

Fig. 2. ***NIPA1-SO*** **negatively regulates** ***NIPA1*** **expression.** (**A**) Immunofluorescence staining of human atherosclerotic arterial tissue samples was used to determine cell-type specific NIPA1 expression. The left-hand images show expression of the cell type-specific markers used to determine cell identity; CD34 for endothelial cells (ECs), LGALS3 for macrophages (MΦs) and α-smooth muscle actin for smooth muscle cells (SMCs). Green fluorescence indicates expression of the indicated markers and thus cell type identity. The central images show NIPA1 staining (red) for the same images as those shown on the left. The merged images on the right demonstrate co-localization of NIPA1 with the indicated cell type markers (example regions of co-localization are indicated using arrows). For all images, nuclei were stained with DAPI (blue). (**B** and **C**) Cultured human umbilical vein endothelial cells (HUVECs), THP-1 cells, and human aortic smooth muscle cells (HASMCs) were transduced with lentiviral vectors encoding *NIPA1-SO* (LV-*NIPA1-SO*) or a mock control lentivirus (LV-Mock). (**B**) The level of *NIPA1* mRNA expression was quantified using RT-PCR. Data is presented following normalization to the endogenous control gene GAPDH and normalization to the LV-Mock samples (n = 5). (**C**) The level of NIPA1 protein in response to lentiviral-mediated overexpression of *NIPA1-SO* in endothelial, monocyte and vascular smooth muscle cells was also assessed using Western blotting, normalizing to β-actin and the LV-mock samples (n = 5). (**D**) The level of NIPA1 protein was examined by Western blotting in response to *NIPA1-SO* knockdown via shRNA (n = 5). Data were normalized to β-actin and control shRNA samples. $^{*}P < 0.05$ by unpaired 2-tailed Student's *t*-test, n = 5 per group. (For interpretation of the references to color in this figure legend, the reader is referred to the web version of this article.)

Of these five proteins, FUBP1 (far upstream element binding protein 1) protein was most abundantly detectable in the *NIPA1-SO* pulldown (Fig. 3A and Appendix Fig. S5). To verify that *NIPA1-SO* could interact with FUBP1, an RNA immunoprecipitation (RIP) assay was performed with an anti-FUBP1 antibody, followed by RT-PCR using the precipitated RNA sample as a template and primers complementary to the *NIPA1-SO* lncRNA sequence. Analysis showed the presence of *NIPA1-SO* in the RNA sample precipitated by the anti-FUBP1 antibody (Fig. 3B), suggesting that *NIPA1-SO* interacts with FUBP1. To investigate which parts of *NIPA1-SO* were likely to be required for the interaction with FUBP1, we performed FUBP1 immunoblotting on different chromatin samples pulled-down using different regions of *NIPA1-SO* as specific probes. The experiment indicated the involvement of the 5́-region (1–303 nt), the middle (276–1056 nt), and 3́-region (960–1451 nt) of *NIPA1-SO* (Appendix Fig. S6 and Fig. 3C and D).

Furthermore, we performed chromatin immunoprecipitation (ChIP) using an anti-FUBP1 antibody, followed by PCR amplification of the precipitated chromatin DNA sample with primers complementary to the *NIPA1* gene. This assay showed enrichment of *NIPA1* in the chromatin precipitated by the anti-FUBP1 antibody (Fig. 3E), suggesting that FUBP1 interacted with *NIPA1*.

To investigate whether the effect of *NIPA1-SO* on NIPA1 expression was dependent upon FUBP1, we transfected HUVECs with a lentivirus that expressed *NIPA1-SO* and a siRNA to knockdown *FUBP1*. Then, we performed Western blot analysis of NIPA1. This experiment showed that the knockdown of *FUBP1* abolished the suppressive effect of *NIPA1-SO* on NIPA1 expression (Fig. 3F), suggesting that *NIPA1-SO* influences NIPA1 expression in a FUBP1-dependent manner. Furthermore, cells that were transfected with the FUBP1 siRNA alone exhibited increased NIPA1 protein levels (Fig. 3F), indicating that FUBP1 negatively regulated NIPA1; taken together with our earlier findings, these data implied that the functionality of FUBP1 was enhanced by *NIPA1-SO*.

NIPA1-SO increases the levels of BMPR2 via NIPA1

Previous studies have shown that NIPA1 interacted with BMPR2 and thereby promoted endocytosis and lysosomal degradation of BMPR2 [13]. Having found that *NIPA1-SO* suppressed *NIPA1* expression, we next investigated whether *NIPA1-SO* could influence BMPR2 levels via NIPA1. Our experiments showed that the lentivirus-mediated overexpression of *NIPA1-SO* in HUVECs, THP-1 cells and HASMCs resulted in an increase in BMPR2 level

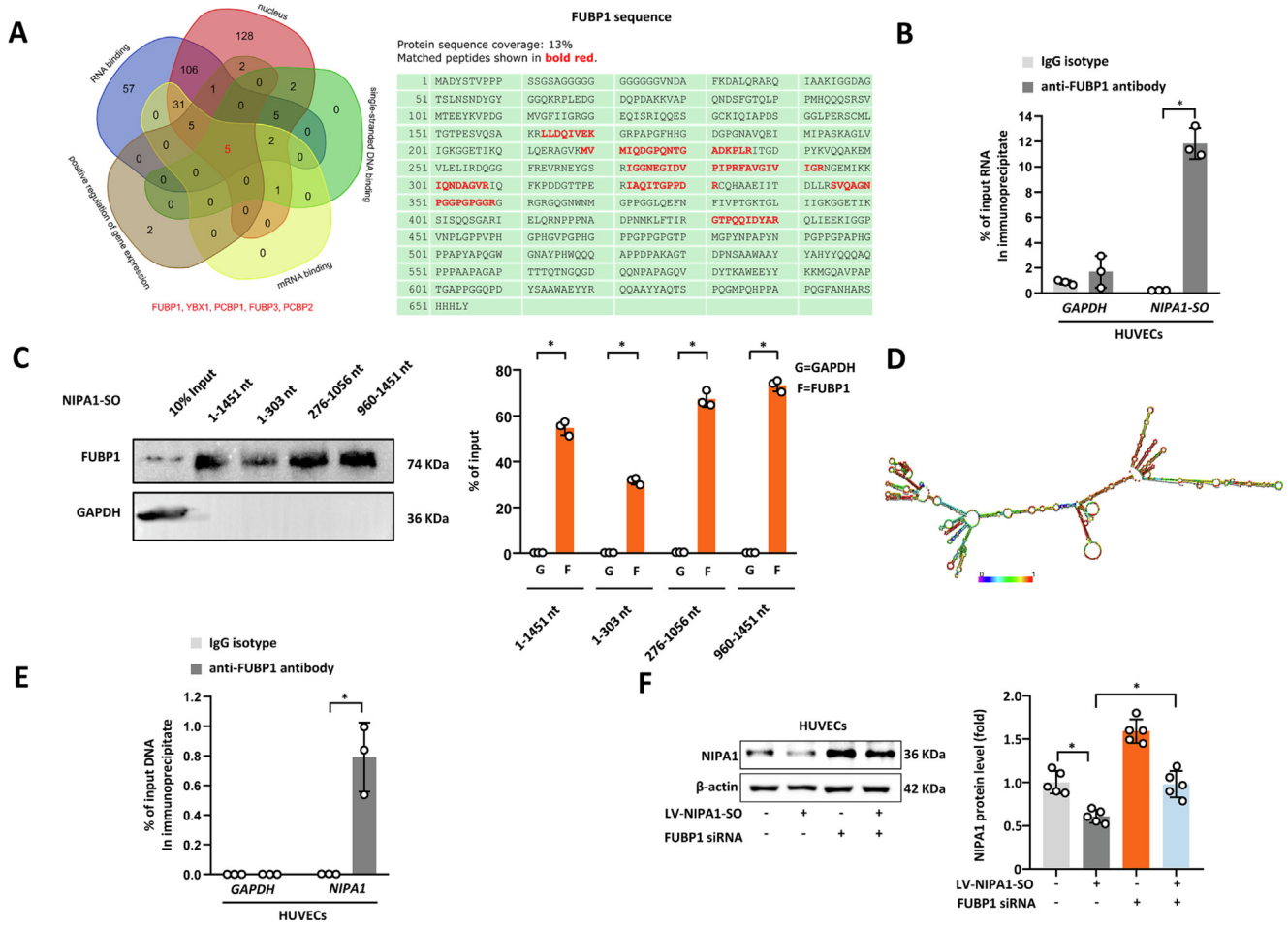

Fig. 3. Negative regulation of *NIPA1* expression by *NIPA1-SO* involves FUBP1. (**A**) Chromatin of cultured HUVECs were pulled down using *NIPA1-SO* RNA probes and subjected to protein mass spectrometry analysis. (**B**) RNA immunoprecipitation was used to determine if the transcription factor FUBP1, identified by mass spectrometry analysis of ChIP samples, interacts with *NIPA1-SO* (n = 3). An anti-FUBP1 antibody was used to immunoprecipitate cellular RNA in HUVECs, and RT-PCR was used to measure the quantity of immunoprecipitated *NIPA1-SO* RNA as a percentage of the input RNA. Primers amplifying the *GAPDH* gene were used as a control for the RT-PCR and an IgG isotype antibody was used as a control for the RNA immunoprecipitation. (**C**) Biotin-labeled full-length (1–1451 nt) and truncated (1–303 nt, 276–1056 nt, and 960–1451 nt) *NIPA1-SO* sequences were prepared by the in vitro transcription method. The labeled sequences were incubated with cell lysate at 4 °C for 3 h and then with streptavidin-conjugated magnetic beads to isolate *NIPA1-SO*-protein complexes, followed by Western blot analysis of FUBP1. n = 3. (**D**) The tertiary structure of *NIPA1-SO* was analyzed by RNAfold, which indicates that *NIPA1-SO* has three functional structure areas: 1–303 nt, 276–1056 nt, and 960–1451 nt, respectively. (**E**) Chromatin immunoprecipitation using an anti-FUBP1 antibody, followed by PCR analysis of *NIPA1*, was used to determine if FUBP1 interacts with the *NIPA1* gene in HUVECs (n = 3). Data are presented as a percentage of input DNA with IgG isotype immunoprecipitation and *GAPDH* PCR used as controls for the immunoprecipitation and PCR, respectively. (**F**) Western blotting was used to determine if *NIPA1-SO*-mediated down-regulation of *NIPA1* is dependent upon FUBP1 using lentiviral overexpression with and without *FUBP1* siRNA in HUVECs (n = 5). Data are presented normalized to β-actin and the untreated control (without lentiviral transduction or siRNA transfection). *$P < 0.05$ by unpaired 2-tailed Student's *t*-test or one-way ANOVA with Tukey's post hoc tests.

(Fig. 4A) while the knockdown of *NIPA1-SO* resulted in a decrease in BMPR2 (Fig. 4B). The effect of *NIPA1-SO* overexpression on BMPR2 level was augmented by the knockdown of *NIPA1* (Fig. 4C), suggesting that *NIPA1-SO* increased BMPR2 levels by reducing NIPA1.

In addition, we investigated whether there was a difference in BMPR2 level between atherosclerotic plaques and normal intimal tissue. Immunohistochemical analysis showed that BMPR2 levels were lower in atherosclerotic plaques than in normal intimal tissues (Fig. 4D). Furthermore, co-localization of BMPR2 with the endothelial cell marker CD34, macrophage marker LGALS3 and the vascular smooth muscle cell marker αSMA was observed (Fig. 4E). Together, these results demonstrated that *NIPA1-SO* upregulated BMPR2 in a NIPA1-dependent manner.

NIPA1-SO and NIPA1 influence THP-1 cell adhesion to HUVECs

It has previously been reported that BMPR2 can inhibit the expression of intercellular adhesion molecule-1 (ICAM1) and vascular cell adhesion molecule-1 (VCAM1) in endothelial cells, thus leading to the reduced adhesion of monocytes to endothelial cells; this is thought to be mediated by the Smad1/5/8-mediated signaling pathway [14,15]. We hypothesized that *NIPA1-SO*, BMPR2 and NIPA1 may influence these events and performed *NIPA1-SO* overexpression and knockdown studies. Our experiments showed that overexpressing *NIPA1-SO* in HUVECs increased the level of pSmad1/5/8 (Fig. 5A) whereas the knockdown of *NIPA1* or *BMPR2* had the opposite effect (Fig. 5B and C). Additionally, we found that the overexpression of *NIPA1-SO* in vascular endothelial cells resulted in the reduced expression of VCAM1 and ICAM1 (Fig. 5D), while the knockdown of *NIPA1-SO* had the opposite effect (Fig. 5E). Furthermore, the effect of *NIPA1-SO* on VCAM1 and ICAM1 expression was attenuated by *BMPR2* knockdown (Fig. 5D and E), suggesting that *NIPA1-SO* inhibits ICAM1 and VCAM1 via the BMPR2-mediated pathway.

Next, we investigated whether *NIPA1-SO*, BMPR2 and NIPA1 could affect monocyte adhesion to endothelial cells. Monocyte adhesion assays showed that the knockdown of *NIPA1-SO* or *BMPR2*

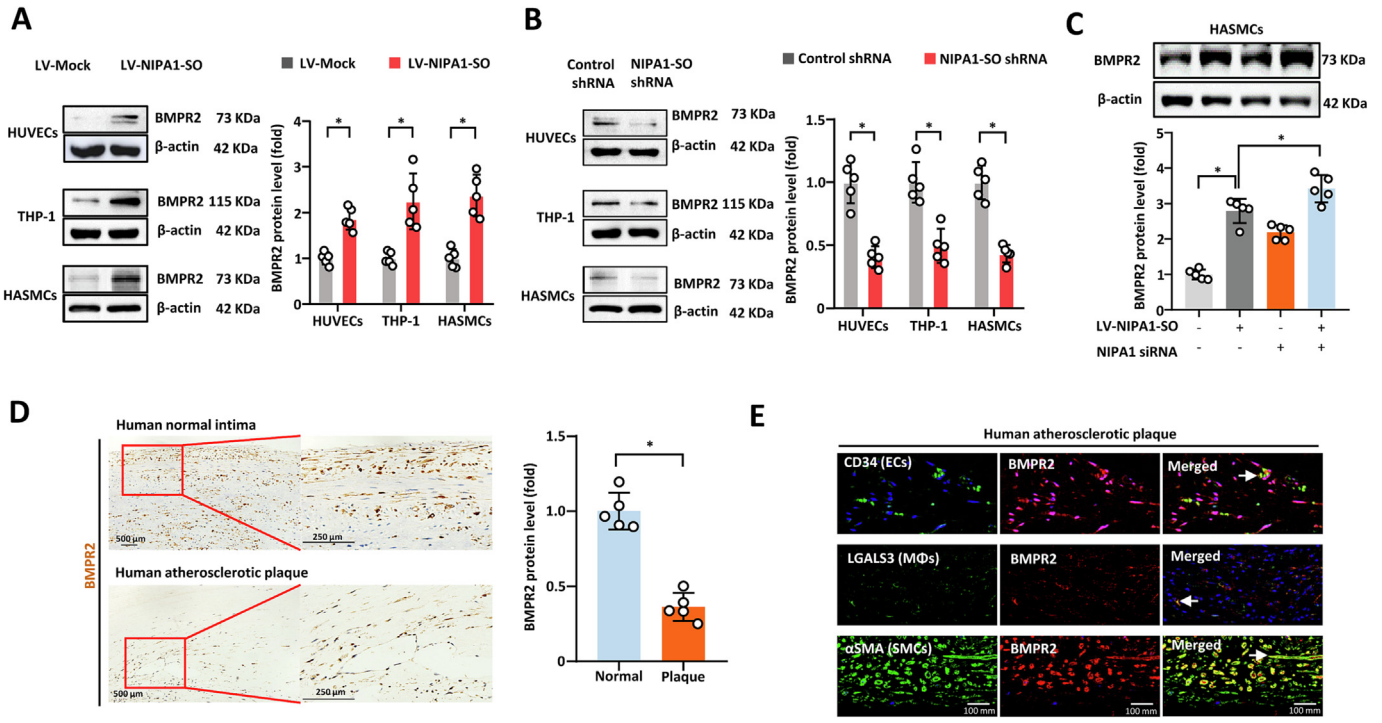

Fig. 4. ***NIPA1-SO*** **increases BMPR2 by reducing** ***NIPA1*** **expression.** (**A**) HUVECs, THP-1 cells, and HASMCs were transduced with *NIPA1-SO*-expressing lentiviral vectors or a control lentivirus (LV-Mock) (n = 5). Western blotting was used to assess BMPR2 protein levels in response to transduction. Data shown are normalized to the mock control samples. (**B**) Knockdown of *NIPA1-SO* in HUVECs, THP-1 cell, and HASMCs, using shRNA, was also used to assess the role of *NIPA1-SO* in BMPR2 expression via Western blot analysis (n = 5). Data were normalized to the control shRNA samples following normalization to β-actin. (**C**) To demonstrate that the regulatory effect of *NIPA1-SO* on BMPR2 is mediated by NIPA1, *NIPA1*-targeting siRNA and overexpression of *NIPA1-SO* was used to assess BMPR2 expression using Western blotting (n = 5). Data for the treatment combinations shown were normalized to β-actin and the control sample (no *NIPA1-SO* overexpression or *NIPA1* knockdown). (**D**) Protein levels of BMPR2 (brown staining) in atherosclerotic plaque tissues or normal tissue samples was assessed via immunohistochemistry (n = 5). Data shown are normalized to the values obtained from normal intimal tissue samples. (**E**) Immunofluroescence staining of atherosclerotic plaque tissue was performed to assess the expression of BMPR2 in different cell types. The left-most images show immunofluorescence staining with cell-type specific markers for endothelial cells (EC; CD34), monocytes (MΦ; LGALS3L) and vascular smooth muscle cells (VSMC; α-smooth muscle actin) with green fluorescence. The center images show corresponding BMPR2 immunofluorescence staining (red) in the three cell types. The images on the right show merged images, demonstrating regions of co-localization between the cell type markers and BMPR2 (as indicated by an arrow). In all immunofluorescence images, staining with DAPI (blue) was used to visualize cell nuclei. (A-E) $^{*}P < 0.05$ by unpaired 2-tailed Student's *t*-test, n = 5 per group. Data are expressed as the mean (±SD) fold differences between the cells transfected with *NIPA1-SO*-expressing lentivirus and cells transfected with the lentivirus vector in three independent experiments. $^{*}P < 0.05$ by unpaired 2-tailed Student's *t*-test. (For interpretation of the references to color in this figure legend, the reader is referred to the web version of this article.)

in HUVECs resulted in increased THP-1 cell adhesion to HUVECs, while the knockdown of *NIPA1* had the opposite effect (Fig. 5F). In contrast, the augmented expression of *NIPA1-SO* caused a reduction in THP-1 cell adhesion to HUVECs and this effect was attenuated by *BMPR2* knockdown (Fig. 5G), suggesting that *NIPA1-SO* inhibits THP-1 cell adhesion to HUVECs in a BMPR2-dependent manner.

NIPA1-SO affects lipid levels in THP-1 cells and HASMCs

There is evidence to suggest that the *BMPR2* gene influences lipid levels [16]. Therefore, we investigated whether *NIPA1-SO* and NIPA1 could affect lipid metabolism and found that in both THP-1 cells (Fig. 6) and HASMCs (Appendix Fig. S7), lentivirus-mediated *NIPA1-SO* overexpression resulted in the increased expression of the cholesterol efflux transporters ATP binding cassette subfamily A member 1 (ABCA1) and ABCG1 (Fig. 6A and Appendix Fig. S7A) and decreased the levels of intracellular cholesterol (Fig. 6B and Appendix Fig. S7B). The shRNA-mediated knockdown of *NIPA1-SO* had the opposite effect (Fig. 6C and D, Appendix Fig. S7C and D). The effect of *NIPA1-SO* on the protein levels of ABCA1 and ABCG1 on intracellular cholesterol level was attenuated by the siRNA-mediated knockdown of *BMPR2* (Fig. 6B and D, Appendix Fig. S7B and D), suggesting that *NIPA1-SO* could influence cellular lipid metabolism in a BMPR2-dependent manner.

NIPA1-SO and NIPA1 affect atherosclerotic plaque formation

Having found that *NIPA1-SO* and NIPA1 were differentially expressed in atherosclerotic plaques (compared to the normal arterial intima) and that the *NIPA1-SO*-FUBP1-NIPA1-BMPR2 pathway influenced adhesion molecule expression, monocyte adhesion to vascular endothelial cells and lipid metabolism, we next investigated whether *NIPA1-SO* and NIPA1 were involved in the development of atherosclerosis.

To test if *NIPA1-SO* influenced atherogenesis, $LDLR^{-/-}$ mice were injected with either an *NIPA1-SO*-expressing lentivirus or a control lentivirus and then fed an atherogenic Western diet for 12 weeks. After this, the atherosclerotic lesions in the two groups were compared. This experiment showed that aortic atherosclerotic lesions in the *NIPA1-SO*-expressing group were smaller, contained less lipid, and had a thicker fibrous cap, than aortic atherosclerotic lesions in the control group (Fig. 7A). An *ex vivo* assay showed that there was a reduction in monocyte adhesion to the aortic endothelium in the *NIPA1-SO*-expressing group when compared with the control group (Fig. 7B).

To test if NIPA1 played a role in atherogenesis, we generated *NIPA1* knock-out mice (on a $LDLR^{-/-}$ background) and fed both $LDLR^{-/-}/NIPA1^{+/+}$ control mice and $LDLR^{-/-}/NIPA1^{-/-}$ mice an atherogenic Western diet for 12 weeks, followed by analyses of atherosclerotic plaque development in the two groups. Analysis

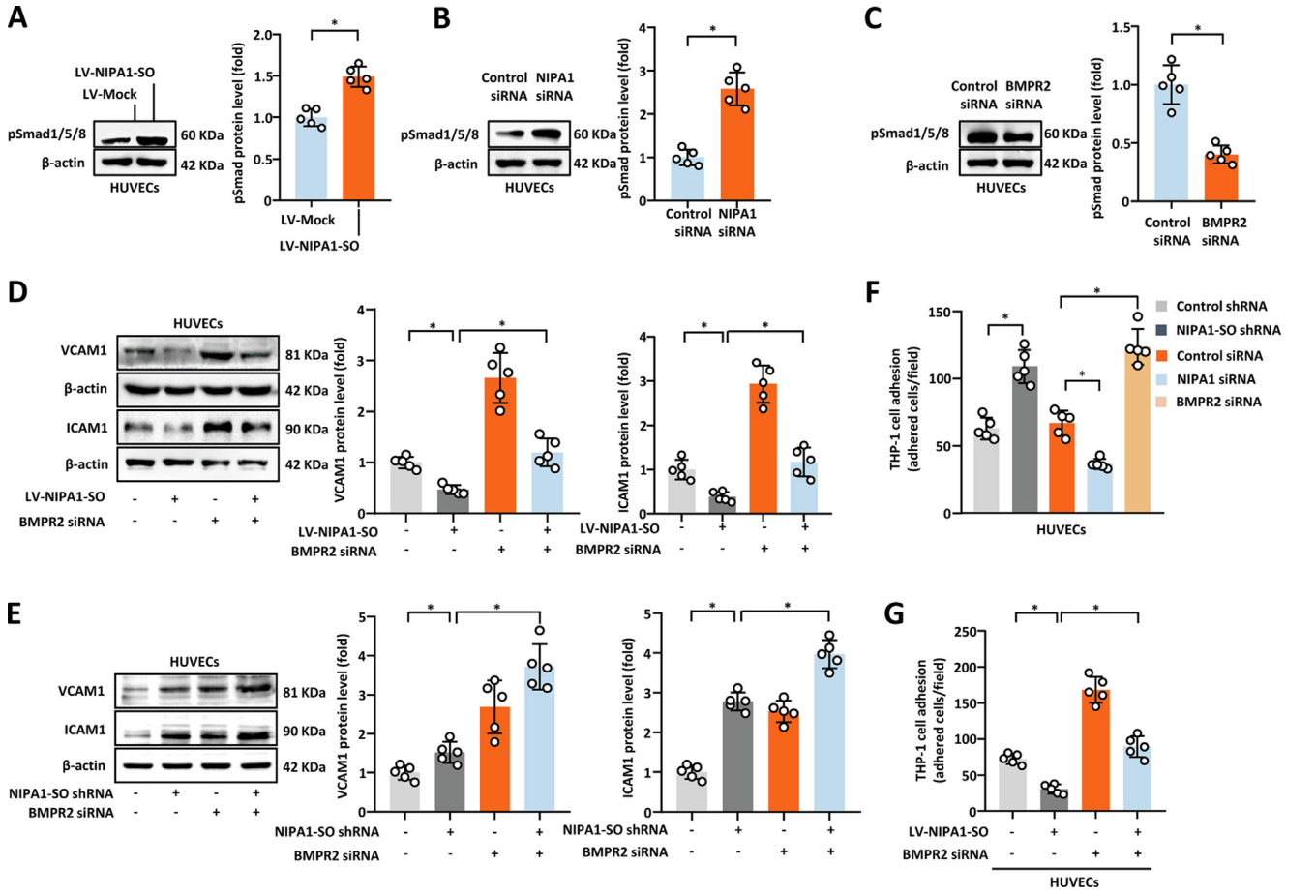

Fig. 5. ***NIPA1-SO*, via NIPA1 signaling, alters expression of adhesion molecules by HUVECs, influencing THP-1 cell adhesion.** (**A** to **C**) The effects of *NIPA1-SO*, NIPA1 and BMPR2 upon pSmad1/5/8 expression were examined via Western blotting and either lentiviral-mediated overexpression (**A**) or knockdown with *NIPA1* siRNA (**B**) or *BMPR2* siRNA (**C**). Data were normalized to β-actin and to control samples (n = 5). (**D**) VCAM1 and ICAM1 expression in response to overexpression of *NIPA1-SO* and/or siRNA-mediated knockdown of *BMPR2* was examined via Western blotting. Data were normalized to β-actin and to control samples (n = 5). (**E**) Knockdown of *NIPA1-SO* and *BMPR2*, both separately and in combination, was used to assess VCAM1 and ICAM1 expression via Western blotting (n = 5). Data are presented following normalization to β-actin and untreated control cells. (**F**) Monocyte adhesion in response to endothelial cell knockdown of *NIPA1-SO*, NIPA1 and BMPR2 was performed. Data are presented as a count of adhered cells per field of the acquired images (n = 5). (**G**) The effect of *NIPA1-SO* overexpression and *BMPR2* knockdown upon monocyte adhesion was also assessed (n = 5). Data shown are a count of the number of adhered cells per image field. $^{*}P < 0.05$ by unpaired 2-tailed Student's *t*-test (**A** to **C**) or one-way ANOVA with Tukey's post hoc tests (**D** to **G**).

found that aortic atherosclerotic lesions were smaller in *LDLR*$^{-/-}$/*NIPA1*$^{-/-}$ mice than *LDLR*$^{-/-}$/*NIPA1*$^{+/+}$ control mice (Fig. 7C). Immunohistochemical analyses of plaque composition showed that atherosclerotic lesions in *LDLR*$^{-/-}$/*NIPA1*$^{-/-}$ mice contained less lipid and fewer monocytes/macrophages but more VSMCs and collagen (indicative of more stable plaques) than atherosclerotic lesions in *LDLR*$^{-/-}$/*NIPA1*$^{+/+}$ control mice (Fig. 7C). Additionally, immunohistochemical analyses of BMPR2, pSmad1/5/8, ICAM1, VCAM1, ABCA1, and ABCG1 showed that compared with atherosclerotic lesions in *LDLR*$^{-/-}$/*NIPA1*$^{+/+}$ control mice, atherosclerotic lesions in *LDLR*$^{-/-}$/*NIPA1*$^{-/-}$ mice had higher levels of BMPR2, pSmad1, ABCA1, and ABCG1, but lower levels of ICAM1 and VCAM1 (Fig. 7D). An *ex vivo* assay demonstrated that there was a reduction in monocyte adhesion to the aortic endothelium in the *LDLR*$^{-/-}$/*NIPA1*$^{-/-}$ group when compared with the *LDLR*$^{-/-}$/*NIPA1*$^{+/+}$ control group (Fig. 7E).

Furthermore, *LDLR*$^{-/-}$/*NIPA1*$^{-/-}$ mice had lower blood levels of ICAM1, VCAM1, triglycerides, total cholesterol, low density lipoprotein cholesterol (LDLc) but higher levels of high-density lipoprotein cholesterol (HDLc) when compared with *LDLR*$^{-/-}$/*NIPA1*$^{+/+}$ control mice (Table S1).

Discussion

In this study, we found that *NIPA1-SO*, a previously uncharacterized lncRNA, played a protective role in the development of atherosclerosis. We found that *NIPA1-SO* down-regulated the expression of the transmembrane protein NIPA1 by interacting with the transcription factor FUBP1 and that there was a decrease of *NIPA1-SO* and an increase of NIPA1 in atherosclerotic plaques. Furthermore, we found that *NIPA1-SO* increased the cellular level of BMPR2 by inhibiting BMPR2 endocytosis by NIPA1, and that *NIPA1-SO* suppressed monocyte adhesion to endothelial cells and intracellular cholesterol accumulation via a BMPR2-dependent pathway. Using a well-established mouse model of atherosclerosis, we demonstrated that augmenting *NIPA1-SO* expression or abolishing NIPA1 resulted in a reduction in the development of atherosclerotic lesions. The pathways uncovered in this study are summarized in Fig. 8.

These findings added to the growing body of evidence demonstrating the importance of lncRNAs in atherosclerosis. Several lncRNAs have been implicated in the pathogenesis of atherosclero-

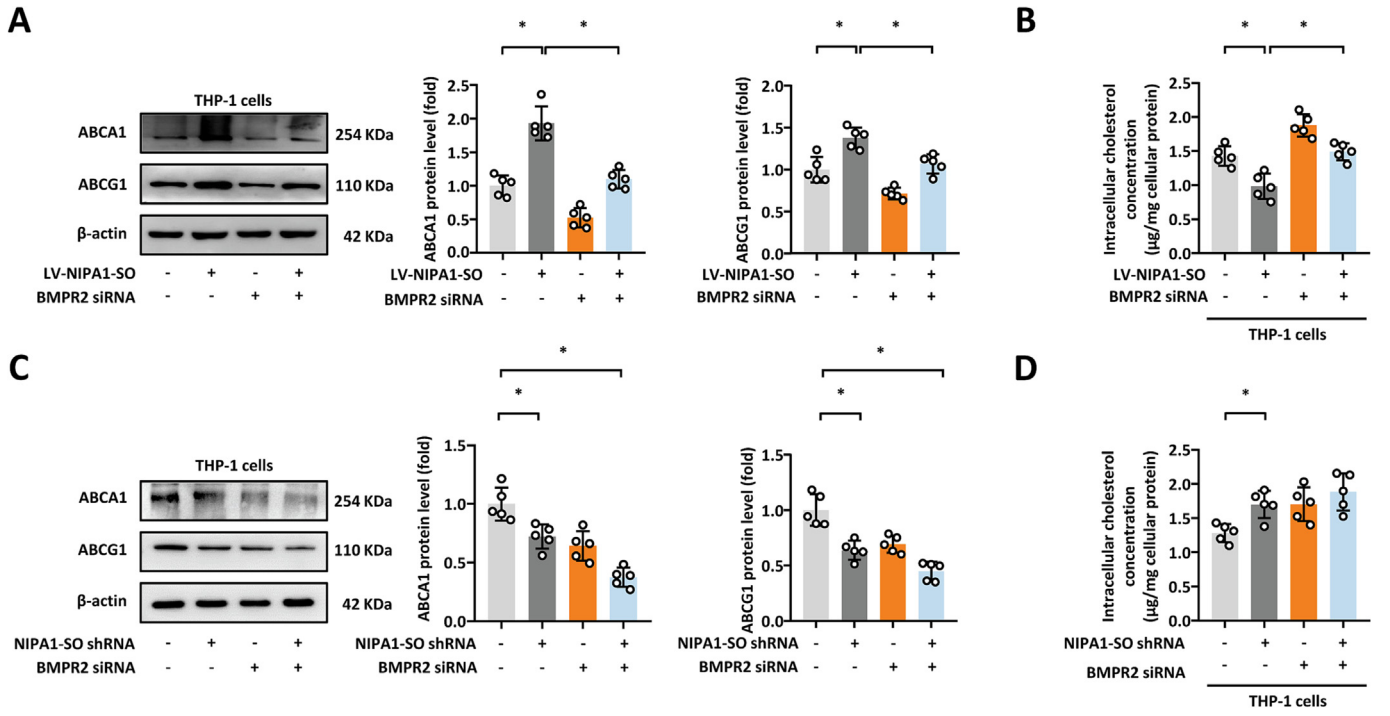

Fig. 6. ***NIPA1-SO*, via BMPR2, increases ABCA1 and ABCG1 levels in THP-1 cells.** (**A** and **B**) Western blotting of the cholesterol efflux-mediators ABCA1 and ABCG1 (**A**) and intracellular cholesterol concentration (**B**), in human monocytes (THP-1 cells) in response to lentiviral overexpression of *NIPA1-SO* and *BMPR2* siRNA knockdown (n = 3). (**C** and **D**) Western blotting of ABCA1 and ABCG1 (**C**) and intracellular cholesterol concentration (**D**), in human THP-1 cells with *NIPA1-SO* shRNA knockdown and *BMPR2* siRNA transfection (n = 3). Data in (**A**) and (**C**) are presented following normalization to β-actin and untreated control cells. *$P < 0.05$ by one-way ANOVA with Tukey's post hoc tests (**A** and **C**) or unpaired 2-tailed Student's *t*-test (**B** and **D**).

sis. For instance, *CDKN2B-AS* (also known as *ANRIL*), is located on chromosome 9p21, the best-known and most widely-replicated coronary artery disease risk locus identified by genome-wide association studies [17]. *CDKN2B-AS* has been shown to modulate the expression of the cell cycle regulators CDKN2B and CDKN2A, thereby influencing vascular smooth muscle cell proliferation and thus contributing to the development of atherosclerotic plaques [18]. LncRNA *CARMN* deficiency has been reported to promote atherosclerosis in mice *in vivo* [19]. Mechanistically, the loss of *CARMN* promotes VSMC proliferation and phenotypic switching [19]. Apart from *CDKN2B-AS* and *CARMN*, the lncRNAs *MeXis* [20], *MALAT1* [21], and *NEXN-AS1* [10] have also been shown to be important players in the development of atherosclerosis. To our knowledge, our present study is the first to reveal that *NIPA1-SO* also plays a (protective) role in atherogenesis.

Non-coding RNAs, including lncRNAs, can be encapsulated into extracellular vesicles and released into the blood and other biofluids in mammals [22]. The non-coding RNAs included in extracellular vesicles become stable because they cannot be degraded by RNA degradation enzyme ribonucleases (RNases), which commonly exist in extracellular fluids [23]. Thus, extracellular lncRNAs represent promising diagnostic and prognostic biomarkers for human diseases. Several lncRNAs have been suggested to serve as diagnostic markers of coronary heart disease. For example, the levels of lncRNA H19 were found to be dramatically elevated in the plasma of patients with coronary heart disease [24]. Furthermore, hyperhomocysteinemia, an independent risk factor for atherosclerosis, induced H19 expression in the aorta of adult C57BL/6 mice [25]. Although we found that *NIPA1-SO* was significantly downregulated in human atherosclerotic plaques, examining the plasma levels of *NIPA1-SO* is of significance in future studies.

The transmembrane protein NIPA1 has been implicated in nervous system development, and mutations in the *NIPA1* gene have been associated with autosomal dominant spastic paraplegia [4,5]. Our study revealed a previously unknown role for this protein in the development of atherosclerosis. Mechanistically, our study showed that NIPA1 enhanced adhesion molecule expression and monocyte adhesion to vascular endothelial cells and indicated that it also promoted a pro-atherogenic lipid profile, with high levels of total cholesterol, LDLc and triglycerides but reduced HDLc. Of relevance, there is reported evidence that NIPA1 physically interacts with BMPR2 and induces the internalization and degradation of BMPR2 [13,15]. We have also shown that NIPA1 negatively regulated the protein levels of BMPR2. Bone morphogenetic protein 2/4 (BMP2/4) was known to play a role in pulmonary arterial smooth muscle cells via BMP2/4-BMPR2-Smad1/5/8 axis [26]. Our results identified that the knockdown of BMPR2 attenuated pSmad1/5/8 signaling in HUVECs. Furthermore, genome-wide association studies have shown a link between genetic variants in the *BMPR2* gene and levels of total cholesterol, LDLc, and HDLc [27,28].

There is little information in the literature about how NIPA1 expression is regulated. Our study indicated that *NIPA1-SO* physically interacted with both the transcription regulator FUBP1 and the *NIPA1* gene, and down-regulated NIPA1 expression in an FUBP1-dependent manner. Interestingly, FUBP1 has been reported to be capable of binding to RNA and DNA molecules and regulating the expression of several other genes [29]. Our study identified *NIPA1-SO* as a novel RNA that FUBP1 could interact with and revealed that the *NIPA1* gene was negatively regulated by FUBP1.

In summary, our study revealed the previously unknown involvement of *NIPA1-SO* and NIPA1 in atherosclerosis, such that *NIPA1-SO* played a protective role against the development of atherosclerotic lesions, whilst NIPA1, which was down-regulated by *NIPA1-SO*, promoted atherogenesis. The findings from our study were pertinent to a better understanding of the pathogenesis of atherosclerosis and suggested that further investigations of

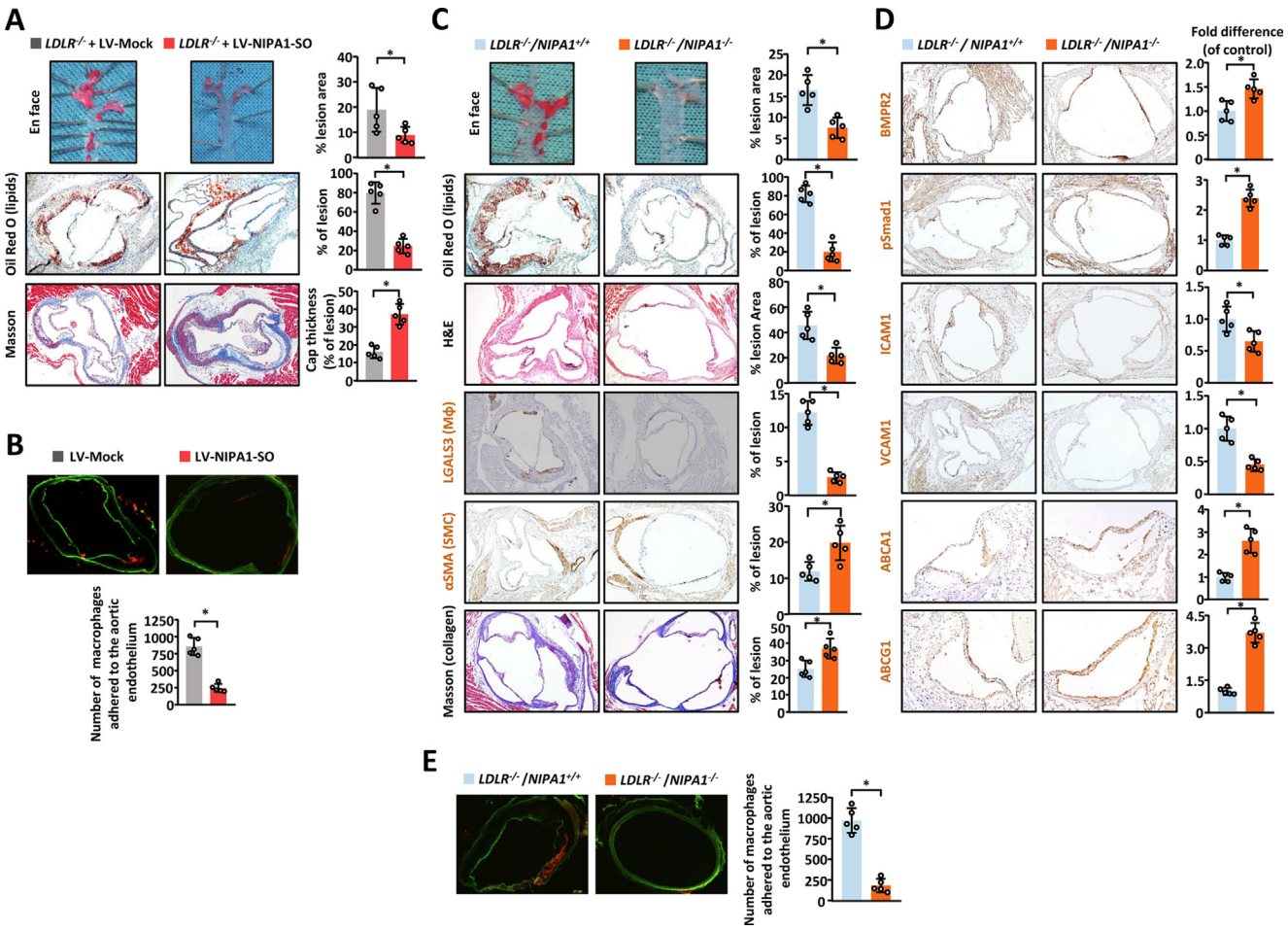

Fig. 7. ***NIPA1-SO*** **and NIPA1 influence atherosclerotic plaque formation in mice** ***in vivo.*** (**A**) En face analysis of aortas from $LDLR^{-/-}/NIPA1^{+/+}$ mice injected with lentivirus to overexpress *NIPA1-SO* or a control lentivirus (LV-Mock) was performed to demonstrate if *NIPA1-SO* is involved in atherogenesis *in vivo* (n = 5). Tissue samples were stained with Oil Red O and the lesion area quantified as a percentage of total en face area. Immunohistochemistry analysis of lesions in $LDLR^{-/-}/NIPA1^{+/+}$ mice overexpressing NIPA1-SO was performed to determine if the composition of atherosclerotic lesions in such mice differs from control mice. Data shown is the % of lesion area positive for Oil Red O (lipid) staining or Masson staining. (**B**) Aortic ring monocyte adhesion assays were performed on $LDLR^{-/-}/NIPA1^{+/+}$ mice injected with *NIPA1-SO* lentiviral particles or a control lentivirus as described in **C** (n = 5). (**C**) En-face dissection and subsequent Oil Red O lipid staining and immunohistochemical analysis of $LDLR^{-/-}/NIPA1^{+/+}$ and $LDLR^{-/-}/NIPA1^{-/-}$ mice fed an atherogenic Western diet for 12 weeks was performed (n = 5). En face aorta samples were stained with Oil Red O (red) to visualize atherosclerotic plaques. Lesion areas, as a percentage of total en face area, are shown. Further analysis of atherosclerotic lesions from the two mouse strains was also performed using Oil Red O staining (quantifying the level of lipid as percentage of the lesion area). Hematoxylin (blue) and eosin (pink) (H&E) staining was also performed to visualize the nuclei and cytoplasm/extracellular matrix (respectively). H&E staining was quantified as a percentage of total lesion area. Immunohistochemistry was used to stain for monocytes (using the marker LGALS3) and smooth muscle cells (using α-smooth muscle actin) as indicated by brown staining. The abundance of these cell types as a percentage of total lesion area is shown. Staining with Masson's trichrome stain was used to determine the quantity of collagen, as a percentage of total lesion area. (**D**) Immunohistochemistry of $LDLR^{-/-}/NIPA1^{+/+}$ and $LDLR^{-/-}/NIPA1^{-/-}$ mice was performed for BMPR2, pSmad1, ICAM1, VCAM1, ABCA1 and ABCG1, with brown staining indicating the presence of the protein of interest. For all immunohistochemistry experiments, the level of each protein, relative to the control ($LDLR^{-/-}/NIPA1^{+/+}$) mice, is presented (n = 5). (**E**) An aortic ring monocyte adhesion assay was performed using $LDLR^{-/-}/NIPA1^{+/+}$ and $LDLR^{-/-}/NIPA1^{-/-}$ mouse aorta samples to determine if *NIPA1* knock-out alters monocyte adhesion to endothelial cells (n = 5). The aortic rings were labeled with calcein-AM and incubated with Dil–labeled mouse peritoneal monocytes. Data presented are the total number of monocytes adhered to the aortic ring for the two groups. Data are presented as the total number of cells adhering to the aortic endothelium. $^{*}P < 0.05$ by unpaired 2-tailed Student's *t*-test. (For interpretation of the references to color in this figure legend, the reader is referred to the web version of this article.)

NIPA1-SO and NIPA1 as potential therapeutic targets for atherosclerosis are warranted.

Materials and methods

Sources and analyses of human tissue samples

The study was conducted following the principles in the Declaration of Helsinki. Twenty human atherosclerotic plaque samples (classified as type V or VI lesions according to the Committee on Vascular Lesions of the Council on Atherosclerosis, American Heart Association [30]), were taken from patients undergoing carotid endarterectomy between May 2013 and May 2014 in the Department of Vascular Surgery, Nanfang Hospital, Southern Medical University, China. None of the patients had received previous treatment for atherosclerosis before surgery. Arteries without macroscopic evidence of atherosclerosis, collected from individuals who died either in a road traffic accident or due to cerebral edema, were used as controls. The study was approved by the Institutional Review Board of Nanfang Hospital, Southern Medical University (Guangzhou, China) and written, informed consent was obtained from participants or relatives of the deceased.

Animals

All animal experiments in this study were approved by the Experimental Animal Center of Guangzhou Medical University and performed following the NIH Guide for the Care and Use of

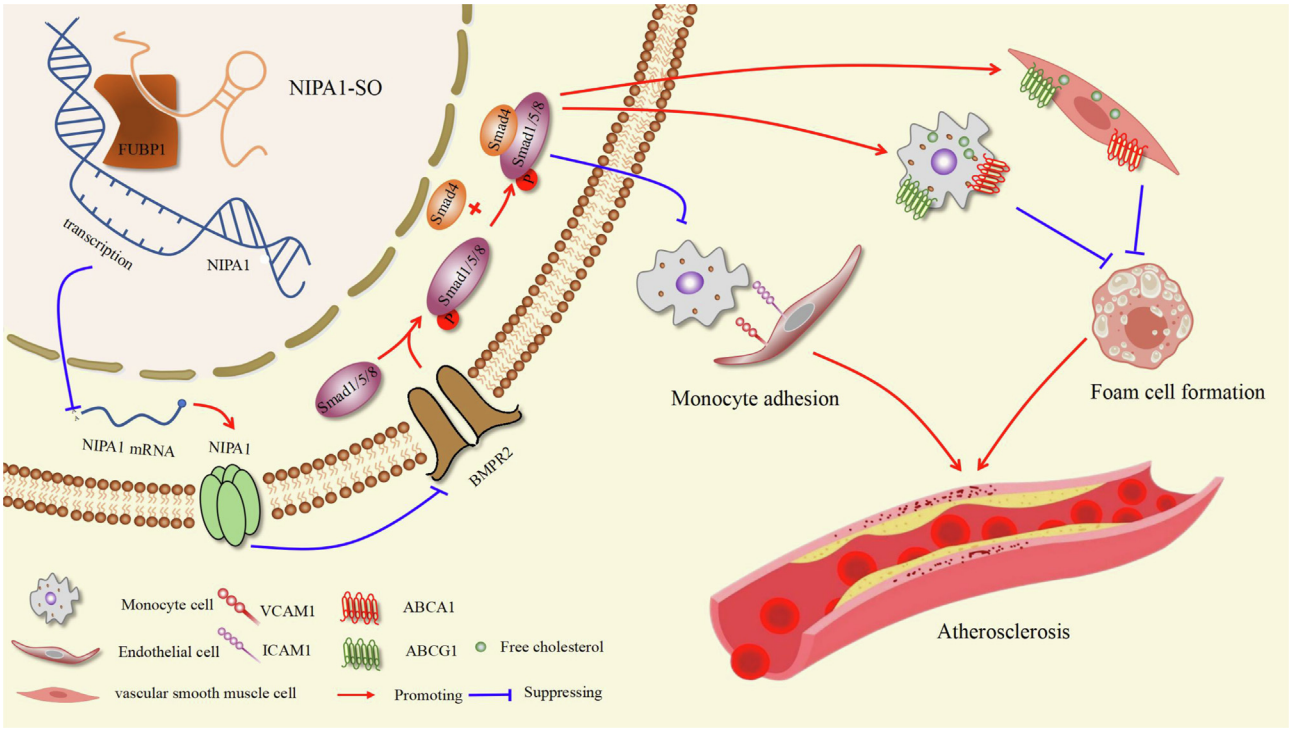

Fig. 8. Schematic diagram of the signalling pathways regulated by *NIPA1-SO*. Our study has uncovered an athero-protective role of the lncRNA *NIPA1-SO*, which, by interacting with a single transcription factor, is capable of inhibiting monocyte adhesion and foam cell formation, two fundamental processes in atherosclerosis. The transcription factor FUBP1 negatively regulates NIPA1 expression; this inhibitory effect is increased by the interaction of *NIPA1-SO* with FUBP1, resulting in lower transcription of NIPA1. A reduction in NIPA1 protein results in increased BMPR2 protein due to a reduction in NIPA1-mediated BMPR2 endocytosis and degradation, leading to higher levels of Smad1/5/8 phosphorylation (pSmad1/5/8), which, through complexation with Smad4, inhibit transcription of the adhesion molecules VCAM1 and ICAM1, reducing monocyte adhesion to endothelial cells. Further, the pSmad1/5/8:Smad4 complex promotes ABCA1 and ABCG1 transcription, both of which promote cholesterol efflux via high-density lipoprotein (HDL) particles, thereby inhibiting foam cell formation.

Laboratory Animals. *LDLR*$^{-/-}$/*NIPA1*$^{-/-}$ mice were generated by crossing *NIPA1*$^{-/-}$ mice (purchased from the Laboratory Animal Center of Peking University (Beijing, China) with *LDLR*$^{-/-}$ mice with a C57BL/6 background (purchased from the Laboratory Animal Center of Peking University (Beijing, China)). Genotype segregation in the offspring followed the expected Mendelian frequency, and we did not observe any developmental/morphological abnormalities. For atherosclerosis development, 8-week-old male *LDLR*$^{-/-}$/*NIPA1*$^{+/+}$ and *LDLR*$^{-/-}$/*NIPA1*$^{-/-}$ mice were placed on an atherogenic Western diet for 12 weeks. After 12 weeks, mice were inhalationally anesthetized with 2% isoflurane and sacrificed by cervical dislocation. 1 ml of blood was collected by cardiac puncture before the mice were sacrificed, and tissues were collected for further analyses.

8-week-old male *LDLR*$^{-/-}$ mice infected with lentivirus to overexpress *NIPA1-SO* (LV-*NIPA1-SO*), or with a negative control lentivirus via tail vein injection, were fed an atherogenic Western diet for 12 weeks. After 12 weeks, the mice in each group were anesthetized as described above and were sacrificed by cervical dislocation. Blood and tissues were collected for further analyses.

Cell culture

Human THP-1 cells, HASMCs and HUVECs were obtained from the American Type Culture Collection (ATCC, Manassas, VA, USA). THP-1 monocytes were maintained in Roswell Park Memorial Institute (RPMI)-1640 medium containing 10% fetal calf serum (FCS). Human vascular endothelial cells and vascular smooth muscle cells were grown in Dulbecco's modified Eagle's medium supplemented with 10% fetal calf serum and 1% penicillin/streptomycin. All cells were incubated at 37 °C in an atmosphere of 5% CO_2. Cells were seeded in 6- or 12-well plates or 60-mm dishes and grown to 60%-80% confluence before use.

En face analysis

Immediately after the mice were sacrificed, the aortas were excised and fixed in 4% paraformaldehyde for quantification of plaque formation using the en face technique. Briefly, after the adventitial tissue was carefully removed, the aorta was opened longitudinally, stained with Oil Red O (0.5% in 60% isopropanol) (Sigma) for 15 min, and pinned to a blue wax surface. En face images were obtained using a stereomicroscope (SZX12; Olympus) equipped with a digital camera (Dxm1200, Nikon) and analyzed using Adobe Photoshop version 7.0 and Scion Image software 4.0. The percentage of the luminal surface area stained by Oil Red O was determined.

Quantification of NIPA1-SO in human atherosclerotic plaques

Total RNA from human atherosclerotic plaques was extracted using TRIzol reagent (Invitrogen). After reverse transcription, real-time PCR was performed on the ABI 7500 Real-Time PCR System (Applied Biosystems) with SYBR Green detection chemistry (Takara Bio). All samples were assayed in triplicate. Data were analyzed using the ΔΔCt method, with *GAPDH* RNA as a reference.

NIPA1-SO copy number analysis

Total RNA was isolated from HUVECs, THP-1 cells, and HASMCs, respectively, and reversed transcribed into cDNA, followed by quantitative PCR of *NIPA1-SO*. The copy number of *NIPA1-SO* RNA

per cell was calculated using a standard curve generated by quantitative PCR using known amounts of *NIPA1-SO* cDNA as templates, the numbers of cell from which RNA samples were extracted, and the Ct values of the *NIPA1-SO* RT-PCR.

Lentivirus production and cell line infection

Human THP-1 cells, HASMCs and HUVECs were cultured as described above. Lentiviral (LV) particles were packaged with constructs expressing either green fluorescent protein only (GFP; LV-Mock), *NIPA1-SO* and GFP (LV-*NIPA1-SO*; for *NIPA1-SO* overexpression), or a shRNA targeting *NIPA1-SO* and GFP (LV-shRNA-*NIPA1-SO*; for *NIPA1-SO* knockdown). GFP expression from all vectors was used to monitor transduction efficiency. The cells were infected with the LV stock at a multiplicity of infection of 100 (THP-1 cells) or 20 (HASMCs and HUVECs) transducing units per cell in the presence of 8 mg/mL of polybrene. The cells were washed with fresh, complete media after 24 h of incubation and GFP-positive cells were counted 96 h post-transduction.

Transfection with small interfering RNA

Small interfering RNAs (siRNAs) targeting *FUBP1*, *NIPA1* and *BMPR2*, and a non-targeting, negative control siRNA, were purchased from Ribo Biotechnology (China). Cells (2×10^6/well) were transfected using Lipofectamine 2000 (ThermoFisher) according to the manufacturer's instructions. After 24- or 48-hours post-transfection, RT-PCR and Western blotting were performed respectively.

Construction of recombinant plasmids

The pIRES2-EGFP and PCR-XL-TOPO vectors (containing *NIPA1*, which were assembled from chemically-synthesized oligonucleotides by PCR) were purchased from Invitrogen. The EcoRI-NIPA1-IRES-EGFP-XhoI fragment was amplified using the PCR-XL TOPO and pIRES2-EGFP vectors as templates for overlap-extension PCR. Gel electrophoresis was performed, and the relevant band was excised from the gel, digested with EcoRI andXhoI in a double-digest, and, incorporated into the pcDNA3.1 (+) vector, and then transformed into competent *Escherichia coli* DH5α cells for further amplification and use. The recombinant plasmids were verified by sequencing and named pcDNA3.1-NIPA1. The plasmid was transfected as indicated using Lipofectamine 2000 (ThermoFisher), according to the manufacturer's instructions.

LncRNA and coding RNA microarray analysis

Total RNA was extracted from either human atherosclerotic plaques (from 3 subjects) or human healthy artery specimens (from 3 subjects) with TRIzol reagent (Invitrogen). The purity and integrity of the total RNA samples were verified by spectrophotometry and gel electrophoresis (Appendix Fig. S8A and B). mRNA was purified from total RNA using mRNA-ONLY Eukaryotic mRNA Isolation Kit (Epicentre) and each mRNA sample transcribed into fluorescent cRNA using a random priming method. Labeled cRNAs were hybridized with Human LncRNA Expression Microarray v3.0 (8×60 K, Arraystar) and scanned using Agilent Scanner G2505C. Data were normalized and analyzed with the use of Agilent Feature Extraction software (version 11.0.1.1) and GeneSpring GX v11.5.1 (Agilent). The expression microarray data have been deposited in the NCBI Gene Expression Omnibus database (GSE97210).

Fluorescent in situ hybridization

FISH was used to investigate *NIPA1-SO* copy number using the PathVysion *NIPA1-SO* RNA probe kit (Vysis) and the Dako Histology FISH Accessory kit. For the Dako Histology kit, the manufacturer's instructions were modified, in order to optimize the technique and decrease the time required for sample processing). Sections were incubated at 56 °C overnight, deparaffinized in two series of xylene, and rehydrated with an ethanol series. Slides were pre-treated with Pre-treatment Solution in a water bath at 97 °C for 10 min. Enzymatic digestion was carried out with Ready-to-Use Pepsin for 3 min at room temperature (endoscopic biopsies) or 6 min at 37 °C (surgical specimens). After dehydration with a graded ethanol series, 10 µl of *NIPA1-SO* probe was applied to each tissue section. The slides and probe were denatured at 80 °C for 5 min and hybridized at 37 °C overnight in a Dako Hybridizer. The next day, the sections were washed with Stringent Wash Buffer at 65 °C for 10 min in a water bath. Then, the slides were dehydrated with a graded ethanol series and mounted using 10 µl of mounting medium containing 4′, 6-diamino-2-phenylindole (DAPI).

Analysis of nuclear versus cytoplasmic ratio of NIPA1-SO

The nuclear and cytoplasmic samples of HUVECs were prepared by nucleocytoplasmic separation kit. Total RNA from nuclear or cytoplasmic was extracted using TRIzol reagent (Invitrogen) according to the manufacturer's instructions. Real-time reverse transcription quantitative PCR (RT-PCR), using SYBR Green detection chemistry, was performed on an ABI 7500 Fast Real-Time PCR system (Applied Biosystems). Finally, the nuclear versus cytoplasmic ratio of *NIPA1-SO* were analyzed.

NIPA1-SO polyadenylation assay

Total RNA from HUVECs were extracted using TRIzol reagent and divided into two groups. In the plus PloyA group, a ploy A tail was added. Subsequently, reverse transcription using oligo dT as primer was carried out in both groups, followed by quantitative PCR using a gene specific upstream primer and oligo dA as a downstream primer.

RNA sequencing

Total RNA was extracted from cultured endothelial cells transduced with either a *NIPA1-SO* expressing lentivirus or the lentivirus vector (n = 3/group), with TRIzol reagent (Invitrogen) according to the manufacturer's protocol, followed by RNA sequencing. The RNA samples were amplified by RT-PCR to libraries with a concentration of >2 nM. The library was sequenced using Illumina NovaSeq 6000 at 6 GigaBases (150 bp ends) per sample. We aligned reads of six samples to the <research species> reference genome using HISAT2 (https://daehwankimlab.github.io/hisat2/, version: hisat2-2.0.4) package [31]. Next, we analyzed the differential expression of lncRNAs using the DESeq2 [32] between two groups. The lncRNAs with a false discovery rate (FDR) below 0.05 and absolute fold change $\geq$ 2 were considered as differentially expressed lncRNAs.

RNA isolation and real-time quantitative PCR analysis

Total RNA from cultured cells was extracted using TRIzol reagent (Invitrogen) according to the manufacturer's instructions. Real-time quantitative PCR (RT-PCR), using SYBR Green detection chemistry, was performed on an ABI 7500 Fast Real-Time PCR system (Applied Biosystems). The expression of *GAPDH* was used as

the internal control for analysis of mRNA level. The expression of U6 RNA was used as the endogenous control for analysis of lncRNA expression from tissues and cells. The PCR primer sequences are shown in Table S2. Melt curve analysis of all RT-PCR products was performed and to confirm production of a single DNA duplex. All samples were measured in triplicate, and the mean Ct value was considered for comparative analysis. Quantitative measurements were determined using the ΔΔCt method, with data normalized to the aforementioned control genes.

Comprehensive identification of RNA binding proteins by mass spectrometry (ChIRP-MS)

Cell harvesting (30×10^8), lysis, disruption, and ChIRP were essentially performed as described by Chu *et al.* [12] with the following modifications: 1) human vascular endothelial cells were crosslinked in 3% formaldehyde for 30 min, followed by 0.125 M glycine quenching for 5 min; 2) hybridization of ChIRP probes (described in Table S3) was initiated late in the day and left to continue overnight; 3) for mass spectrometry experiments, lysates were pre-cleared by incubation with 30 µl washed beads per ml of lysate at 37 °C for 30 min with shaking. Prior to hybridization, beads were removed from the lysates twice using a magnetic stand; 4) for RNase control, lysates were pooled first and aliquoted into two equal amounts. 1/1000 vol of 10 mg/ml RNase A (Sigma) was added to the RNase control sample and both control and non-treated samples were incubated at 37 °C for 30 min with mixing prior to the hybridization steps. RNA extraction was performed from a small aliquot of post-ChIRP beads as described [12]. For protein elution, beads were collected with a magnetic stand, resuspended in biotin elution buffer (12.5 mM biotin (Invitrogen), 7.5 mM HEPES pH 7.5, 75 mM NaCl, 1.5 mM EDTA, 0.15% SDS, 0.075% sarkosyl, and 0.02% sodium deoxycholate), mixed at room temperature for 20 min, and then at 65 °C for 10 min. The eluate was transferred to a fresh tube and the beads were eluted again. The two eluates were pooled, and residual beads were removed again using the magnetic stand. ¼ total volume of 10% trichloroacetic acid was added to the eluate, and after thorough mixing, proteins were precipitated at 4 °C overnight. The next day, proteins were pelleted at 16,000 *g* at 4 °C for 30 min. Supernatant was carefully removed from the tubes and protein pellets were washed once with cold acetone, and pelleted again at 16,000 *g* at 4 °C for 5 min. The acetone was removed and the pellets were briefly centrifuged again and, after removal of residual acetone, left to air-dry for 1 min at room temperature. The protein pellet was then immediately dissolved in appropriate volumes of 1 × Laemmli buffer and boiled at 95 °C for 30 min with occasional mixing to reverse the cross-links. Final protein samples were size-separated in bis-tris SDS-PAGE gels (Invitrogen) for Western blots or mass spectrometry.

Chromatin immunoprecipitation (ChIP) assays

ChIP analysis of human vascular endothelial cells using anti-FUBP1 antibody (Abcam, ab213525) was performed using the protocol provided by the ChIP kit manufacturer (Pierce Agarose ChIP Kit, Thermo Scientific). Immunoprecipitated DNA was analyzed on a LightCycler 480 (Roche) using LightCycler 480 SYBR Green I Master Mix (Roche). PCR primer sequences are shown in Table S4.

RNA immunoprecipitation (RIP)

Nuclear extracts from cultured human vascular endothelial cells (HUVECs) were prepared and incubated with anti-FUBP1 antibody (Abcam, ab213525) or a non-specific mouse IgG, at 4 °C overnight. Protein G Plus Protein A agarose beads (Calbiochem) were then added and the mix was incubated at 4 °C for 2 h, follow by centrifugation to pellet the beads. After washing and elution, immunoprecipitated RNA was extracted with the use of TRIzol reagent (Takara Bio) and RT-PCR was the performed to detect *NIPA1-SO* binding to immunoprecipitated FUBP1, followed by agarose gel electrophoresis. The PCR primer sequences are shown in Table S5.

RNA pulldown

Biotin-labeled full-length (1–1451 nt) and truncated (1–303 nt, 276–1056 nt, and 960–1451 nt) *NIPA1-SO* sequences were prepared by the in vitro transcription method. The labeled sequences were incubated with cell lysate at 4 °C for 3 h and then with streptavidin-conjugated magnetic beads to isolate *NIPA1-SO*-protein complexes, followed by Western blot analysis of FUBP1.

Intracellular cholesterol concentration assay

Intracellular cholesterol concentration was extracted using a mixture of chloroform, isopropanol and NP-40 in the 7:11:0.1 ratio and measured with the use of Cholesterol/Cholesteryl Ester Quantitation Assay kit (Abcam, ab65359). The results were expressed as microgram cholesterol/mg cellular protein.

Analyses of aortic sinus atherosclerotic lesions

The upper portion of the heart and proximal aorta were obtained from sacrificed mice, embedded in Optimal Cutting Temperature compound (Fisher), and stored at −80 °C. Serial 10 µm thick cryosections of aorta, beginning at the aortic root, were collected for a distance of 400 µm. Sections were stained with either Oil Red O, hematoxylin and eosin, or Masson's trichrome, or were immunostained for either LGALS3, αSMA, BMPR2, pSmad1/5/8, ICAM1, VCAM1, ABCA1, or ABCG1. Digitized color images of stained sections were analyzed using Image-Pro Plus image analysis software (Media Cybernetics, Rockville, MD, USA).

Immunohistochemistry

Sections (4 µm thick) of formalin-fixed, paraffin-embedded human atherosclerotic plaques and normal arterial wall specimens, mouse atherosclerotic plaque specimens from mice overexpressing LV-*NIPA1-SO* or arterial wall specimens from mice transduced with a negative control lentivirus, were subjected to immunohistochemistry, comprising gradient alcohol dehydration, antigenic retrieval, 3% hydrogen peroxide blocking and non-immune sheep serum blocking. The human sections were incubated with an anti-NIPA1 antibody (Abcam, ab121744). The mouse-derived sections were incubated with anti-galectin 3 (LGALS3) antibody (Abcam, ab2785), anti-alpha smooth muscle actin (αSMA) antibody (Abcam, ab32575), anti-anti-ABCA1 antibody (Abcam, ab18180), anti-ABCG1 antibody (Abcam, ab217023), anti-ICAM1 antibody (Abcam, ab119871), anti-VCAM1 antibody (Abcam, ab134047), and anti-BMPR2 antibody (Abcam, ab130206), anti-pSmad1 (S187) antibody (Abcam, ab73211), respectively. Negative controls were performed by incubating samples with non-immune sheep serum. The immunohistochemical staining was visualised using a colorimetric kit (Gene Tech, GK500705) and images were acquired using an Olympus BX50 microscope with a digital color camera and analyzed using Image J (version 1.8.0).

Immunohistofluorescence analysis

Sections (4 µm thick) formalin-fixed, paraffin-embedded human atherosclerotic plaques and normal arterial wall specimens, respectively, were incubated with an anti-NIPA1 antibody (Abcam,

ab121744) together with a mouse antibody for either human CD34 (Abcam, ab8536), human αSMA (Abcam, ab7817), or human CD68 (Abcam, ab955), followed by incubation with a Texas red–conjugated anti-rabbit secondary antibody (Abcam, ab6719) and an FITC-conjugated anti-mouse secondary antibody (Abcam, ab6785). Nuclei were counterstained with DAPI. The fluorescent images were acquired using an Olympus BX50 microscope with a digital color camera and analyzed using Image J (version 1.8.0).

Fluorescence confocal microscopy

Human vascular endothelial cells (HUVECs) were seeded on coverslips, fixed with paraformaldehyde, permeabilized with 0.25% Triton X-100, and then incubated with a digoxin-labeled probe for detecting NIPA1-SO. Thereafter, cells were incubated with a DyLight 594-conjugated IgG fraction (Abcam, ab96873) coupled with a monoclonal mouse anti-digoxin antibody (Abcam, ab116590). In a separate experiment, fixed and permeabilized HUVECs were incubated with an anti-NIPA1 antibody (Abcam, ab121744) and subsequently with a fluorophore-conjugated goat anti-rabbit antibody (Abcam, ab6717). Nuclei were counterstained with DAPI. Cells were imaged using an Olympus FV1000 confocal laser scanning microscope.

Monocyte adhesion to aortic rings

Aortas were isolated from *LDLR* $^{-/-}$/*NIPA1* $^{+/+}$ and *LDLR* $^{-/-}$/*NIPA1* $^{-/-}$ mice and placed into a Petri dish filled with cold, sterile PBS to keep the tissue moist. The aorta samples were dissected to remove extraneous tissue (such as fat tissue) and then sliced into 1 mm rings. The aortic rings were labeled with calcein-AM, then washed with PBS and then incubated with Dil–labeled mouse peritoneal monocytes (isolated from C57BL/6 mice) for 2 h at 37 °C with agitation at 90 rpm. Subsequently, the aortic rings were washed with PBS and embedded cross-wise in optimum cutting temperature medium, snap-frozen, and stored at − 80 °C. Multiple 10 μm sections were cut using a cryotome, fixed in formalin, and analyzed using fluorescence microscopy. Images were captured and analyzed to determine the number of macrophages that had adhered to the luminal endothelium of the aortic rings.

Western blot analyses

Protein extracts from cultured cells and tissue samples were prepared in accordance with established methods. Protein extracts were separated using 10% sodium dodecyl sulfate polyacrylamide gel electrophoresis and then subjected to Western blot analyses using rabbit polyclonal anti-NIPA1, -FUBP1, -BMPR2 antibodies (Proteintech Group), rabbit polyclonal anti-pSmad1/5/8 antibodies (Abcam) and rabbit polyclonal anti-ICAM-1, anti-VCAM-1, and anti-β-actin antibodies (Santa Cruz Biotechnologies). Chemiluminescent visualization was performed using the ECL Plus Western Blot Detection System (Amersham Biosciences).

Cell adhesion assay

HUVECs were plated into 6-well plates (1×10^5/well) to and cultured at 37°C/5% CO_2 to form a confluent monolayer. The cells were washed with medium and incubated with fresh growth medium in the presence or absence of TNF-α (10 ng/ml) for 8 h. THP-1 monocytes (at 2×10^5 cells/ml) stained with 5 μM carboxyfluorescein succinimidyl ester (Genecopoeia) was then added to each well and incubated for 30 min under standard culture conditions (37 °C, 5% CO_2). After 4–6 h of incubation, non-adherent monocytes were gently removed by washing twice with PBS. Monocyte adhesion was quantified by counting the number of adhered monocytes with green fluorescence using a fluorescence microscope. Experiments were repeated at least three times.

Measurement of serum biochemical parameters

The serum concentrations of ICAM-1 and VCAM-1 in mice were measured by ELISA kits with an anti-ICAM1 antibody (Abcam ab100688) and an anti-VCAM1 antibody (Abcam, ab201278), respectively. The total cholesterol (TC), triglyceride (TG), high density lipoprotein cholesterol (HDL-C) and low density lipoprotein cholesterol (LDL-C) levels in the serum were measured using a Roche automatic biochemical analyzer (Roche, C7500).

Statistical analyses

Data were analyzed using Statistical Package for the Social Sciences (SPSS) software (version 13.0). Normally distributed data are presented as mean ± SD or median (interquartile range in skewed-distributed data), unless otherwise indicated. Continuous variables were analyzed by one-way ANOVA with Bonferroni's correction applied for multiple comparisons, or by unpaired 2-tailed Student's *t*-test, with $P < 0.05$ considered significant. The correlations between selected protein levels and biochemical parameters were analyzed using Pearson's or Spearman's correlation, with $P < 0.05$ considered significant.

Data and materials availability

The data, analytic methods, and study materials will be/have been made available to other researchers for purposes of reproducing the results or replicating the procedure. The supplementary materials have been uploaded to Nutstore. The web hyperlink is provided below. https://www.jianguoyun.com/p/DZrlZS4QsPHhChiZqMsEIAA.

Declaration of Competing Interest

The authors declare that they have no known competing financial interests or personal relationships that could have appeared to influence the work reported in this paper.

Acknowledgments

This work was supported by the National Natural Sciences Foundation of China (Grant numbers: 82072335, 81871701, 82070466, 81800364, and 81974046), the Natural Science Fund of Guangdong (Grant numbers: 2020B1515020013, 2018A030313533, and 2017A030313535), Guangzhou Women and Children' s Medical Center (Grant number: GWCMC2020-6-010), and Fujian Joint Funds for the Innovation of Science and Technology (Grant number: 2018Y9099). SY thanks the support of the British Heart Foundation (Grant numbers: RG/16/13/32609, RG/19/9/34655, SP/19/2/344612, PG/16/9/31995, and PG/18/73/34059). This work falls under the portfolio of research conducted within the NIHR Leicester Biomedical Research Centre.

Appendix A. Supplementary material

Supplementary data to this article can be found online at https://doi.org/10.1016/j.jare.2023.01.017.

References

[1] Batista PJ, Chang HY. Long noncoding RNAs: cellular address codes in development and disease. Cell 2013;152:1298–307.
[2] Uchida S, Dimmeler S. Long noncoding RNAs in cardiovascular diseases. Circ Res 2015;116:737–50.
[3] Rudenskaya GE, Kadnikova VA, Bessonova LA, Sparber PA, Kurbatov SA, Mironovich OL, et al. Autosomal dominant spastic paraplegias. Zh Nevrol Psikhiatr Im S S Korsakova. 2021;121:75–87.
[4] Rainier S, Chai JH, Tokarz D, Nicholls RD, Fink JK. NIPA1 gene mutations cause autosomal dominant hereditary spastic paraplegia (SPG6). Am J Hum Genet 2003;73:967–71.
[5] Reed JA, Wilkinson PA, Patel H, Simpson MA, Chatonnet A, Robay D, et al. A novel NIPA1 mutation associated with a pure form of autosomal dominant hereditary spastic paraplegia. Neurogenetics 2005;6:79–84.
[6] Goytain A, Hines RM, El-Husseini A, Quamme GA. NIPA1(SPG6), the basis for autosomal dominant form of hereditary spastic paraplegia, encodes a functional Mg2+ transporter. J Biol Chem 2007;282:8060–8.
[7] Vanlerberghe C, Petit F, Malan V, Vincent-Delorme C, Bouquillon S, Boute O, et al. 15q11.2 microdeletion (BP1-BP2) and developmental delay, behaviour issues, epilepsy and congenital heart disease: a series of 52 patients. Eur J Med Genet 2015;58:140–7.
[8] Wang D, Zhu ZL, Lin DC, Zheng SY, Chuang KH, Gui LX, et al. Magnesium supplementation attenuates pulmonary hypertension via regulation of magnesium transporters. Hypertension 2021;77:617–31.
[9] Bai HL, Lu ZF, Zhao JJ, Ma X, Li XH, Xu H, et al. Microarray profiling analysis and validation of novel long noncoding RNAs and mRNAs as potential biomarkers and their functions in atherosclerosis. Physiol Genomics 2019;51:644–56.
[10] Hu YW, Guo FX, Xu YJ, Li P, Lu ZF, McVey DG, et al. Long noncoding RNA NEXN-AS1 mitigates atherosclerosis by regulating the actin-binding protein NEXN. J Clin Invest 2019;129:1115–28.
[11] Dong XH, Lu ZF, Kang CM, Li XH, Haworth KE, Ma X, et al. The long noncoding RNA RP11-728F11.4 promotes atherosclerosis. Arterioscler Thromb Vasc Biol 2021;41:1191–204.
[12] Chu C, Qu K, Zhong FL, Artandi SE, Chang HY. Genomic maps of long noncoding RNA occupancy reveal principles of RNA-chromatin interactions. Mol Cell 2011;44:667–78.
[13] Wang X, Shaw WR, Tsang HT, Reid E, O'Kane CJ. Drosophila spichthyin inhibits BMP signaling and regulates synaptic growth and axonal microtubules. Nat Neurosci 2007;10:177–85.
[14] Kim CW, Song H, Kumar S, Nam D, Kwon HS, Chang KH, et al. Anti-inflammatory and antiatherogenic role of BMP receptor II in endothelial cells. Arterioscler Thromb Vasc Biol 2013;33:1350–9.
[15] Tsang HT, Edwards TL, Wang X, Connell JW, Davies RJ, Durrington HJ, et al. The hereditary spastic paraplegia proteins NIPA1, spastin and spartin are inhibitors of mammalian BMP signalling. Hum Mol Genet 2009;18:3805–21.
[16] Feng J, Gao J, Li Y, Yang Y, Dang L, Ye Y, et al. BMP4 enhances foam cell formation by BMPR-2/Smad1/5/8 signaling. Int J Mol Sci 2014;15:5536–52.
[17] Samani NJ, Erdmann J, Hall AS, Hengstenberg C, Mangino M, Mayer B, et al. Genomewide association analysis of coronary artery disease. N Engl J Med 2007;357:443–53.
[18] Lo Sardo V, Chubukov P, Ferguson W, Kumar A, Teng EL, Duran M, et al. Unveiling the role of the most impactful cardiovascular risk locus through haplotype editing. Cell 2018;175(1796–1810):e1720.
[19] Vacante F, Rodor J, Lalwani MK, Mahmoud AD, Bennett M, De Pace AL, et al. CARMN loss regulates smooth muscle cells and accelerates atherosclerosis in mice. Circ Res 2021;128:1258–75.
[20] Sallam T, Jones M, Thomas BJ, Wu X, Gilliland T, Qian K, et al. Transcriptional regulation of macrophage cholesterol efflux and atherogenesis by a long noncoding RNA. Nat Med 2018;24:304–12.
[21] Cremer S, Michalik KM, Fischer A, Pfisterer L, Jae N, Winter C, et al. Hematopoietic deficiency of the long noncoding RNA MALAT1 promotes atherosclerosis and plaque inflammation. Circulation 2019;139:1320–34.
[22] Gruner HN, McManus MT. Examining the evidence for extracellular RNA function in mammals. Nat Rev Genet 2021;22:448–58.
[23] Sorrentino S. Human extracellular ribonucleases: multiplicity, molecular diversity and catalytic properties of the major RNase types. Cell Mol Life Sci 1998;54:785–94.
[24] Xiong G, Jiang X, Song T. The overexpression of lncRNA H19 as a diagnostic marker for coronary artery disease. Rev Assoc Med Bras 1992;2019(65):110–7.
[25] Glier MB, Ngai YF, Sulistyoningrum DC, Aleliunas RE, Bottiglieri T, Devlin AM. Tissue-specific relationship of S-adenosylhomocysteine with allele-specific H19/Igf2 methylation and imprinting in mice with hyperhomocysteinemia. Epigenetics 2013;8:44–53.
[26] Meng L, Liu X, Teng X, Yuan W, Duan L, Meng J, et al. DAN plays important compensatory roles in systemic-to-pulmonary shunt associated pulmonary arterial hypertension. Acta Physiol (Oxf) 2019;226:e13263.
[27] Hoffmann TJ, Theusch E, Haldar T, Ranatunga DK, Jorgenson E, Medina MW, et al. A large electronic-health-record-based genome-wide study of serum lipids. Nat Genet 2018;50:401–13.
[28] Klarin D, Damrauer SM, Cho K, Sun YV, Teslovich TM, Honerlaw J, et al. Genetics of blood lipids among ~300,000 multi-ethnic participants of the Million Veteran Program. Nat Genet 2018;50:1514–1523.
[29] Zhang J, Chen QM. Far upstream element binding protein 1: a commander of transcription, translation and beyond. Oncogene 2013;32:2907–16.
[30] Stary HC, Chandler AB, Dinsmore RE, Fuster V, Glagov S, Insull W, Jr., et al. A definition of advanced types of atherosclerotic lesions and a histological classification of atherosclerosis. A report from the Committee on Vascular Lesions of the Council on Arteriosclerosis, American Heart Association. Circulation 1995;92:1355–1374.
[31] Kim D, Paggi JM, Park C, Bennett C, Salzberg SL. Graph-based genome alignment and genotyping with HISAT2 and HISAT-genotype. Nat Biotechnol 2019;37:907–15.
[32] Love MI, Huber W, Anders S. Moderated estimation of fold change and dispersion for RNA-seq data with DESeq2. Genome Biol 2014;15:550.